

NUMERICAL STUDY ON HEAT TRANSFER AND FLOW RESISTANCE CHARACTERISTICS OF MULTI-HEAD TWISTED SPIRAL TUBE

by

Zhiqun ZHENG^a, Fayi YAN^{a*}, and Lei SHI^b

^a School of Mechanical and Electronic Engineering, Shandong Jianzhu University, Shandong, China

^b School of Automotive Studies, Tongji University, Shanghai, China

Original scientific paper

<https://doi.org/10.2298/TSCI210224206Z>

A numerical calculation model of multihead twisted spiral tube was established. In the range of Reynolds number from 5000 to 35000, the influence of different twisted structure on the flow and heat transfer characteristics of the multihead twisted spiral tube was studied by numerical calculation. Numerical calculation results indicate that the Nusselt number and friction coefficient increase with the increase in the ratio of outside and inside diameter of the cross-section, the increase in the number of twisted nodes, and the increase in the number of twisted spiral tube heads. Under the condition of the same spiral structure and the same hydraulic diameter, the heat transfer performance of the multihead twisted spiral tube is better than that of the spiral smooth tube. In addition, through artificial neural network analysis, the ratio of outside and inside diameter of the cross-section, number of twisted nodes, and the number of twisted spiral tube heads were optimized to promote the comprehensive heat transfer performance. The performance evaluation criterion is the highest when the ratio of outside and inside diameter of the cross-section is 25/22.5, the number of twisted nodes is 3, and the number of twisted spiral tube heads is 3, which is 1.849 of the spiral smooth tube.

Key words: multihead twisted spiral tube, heat transfer, numerical simulation, artificial neural network

Introduction

Heat exchangers are widely used in petroleum, chemical, energy, and other fields. With the continuous development of industrial technology, the mechanism of enhanced heat transfer in heat exchangers has been extensively studied to save energy and improve heat exchange efficiency [1]. The enhanced heat transfer mechanism [2] is generally divided into active enhanced heat transfer and passive enhanced heat transfer. Among them, the passive enhanced heat exchange does not use auxiliary power. The turbulence in the heat exchanger is improved through the structure and arrangement of the heat exchanger to enhance heat exchange.

The multihead twisted spiral tube (MTST) heat exchanger has both a spiral structure and a twisted tube structure. The spiral structure can generate counter-rotating vortex through centrifugal force to enhance heat exchange. Mishra *et al.* [3] studied the pressure changes of Newtonian fluid and non-Newtonian fluid-flowing through the spiral tube, and the calculation

* Corresponding author, e-mail: yanfayi@sdjzu.edu.cn

formulas of the friction factor in the spiral tube were given based on the experimental data. Cioncolini *et al.* [4] experimentally studied the turbulent flow process in adiabatic spiral coils. The results showed that when the smoothing effect of turbulence is equivalent to the triggering effect of the secondary flow, the enhancement effect of the secondary flow triggering will be cancelled. Gupta *et al.* [5] experimentally investigated the influence of coil pitch and coil diameter on the friction factor during the flow of spiral coils. The calculation formula of the corresponding friction factor under different Germano number was proposed.

The heat transfer enhanced mechanism of twisted tubes are similar with spiral corrugated tubes [6-11] and threaded grooved tubes [12]. Secondary flow is generated by variety of tube shape, which periodically destroys the heat transfer boundary-layer of the tube wall. Besides, twisted tubes generate more wall heat exchange area than smooth tubes, so the heat exchange is more sufficient. Khoshvaght *et al.* [13] compared the flow and heat transfer characteristics of corrugated channels, twisted channels, and corrugated twisted channels with a rectangular cross-section. The calculation results showed that the hydrothermal performance of corrugated channels and corrugated twisted channels decrease with the increase of Reynolds number. The influence of the geometric structure of the three-lobed twisted tube on the flow and heat transfer characteristics was experimentally studied by Tang *et al.* [14]. The experimental results showed that the larger the outer circle diameter, the higher the Nusselt number and the larger the friction factor. The principle of field synergy was applied to analyze the enhancing heat transfer mechanism of the elliptical twisted tube by Yang *et al.* [15]. Synergy between the velocity vector and temperature gradient was improved, which enhanced heat transfer efficiency. Kareem *et al.* [16] analyzed the flow and heat transfer characteristics of water in a three-head spiral bellows under low Reynolds number, and the calculation data was compared with a smooth tube. The results showed that the enhanced heat transfer range is 2.4~3.7 times, and friction factor is 1.7~2.4 times of smooth tube. Jin *et al.* [17] studied the influence of the geometric parameters, flow characteristics and other factors of the six-start spiral tube on its heat transfer characteristics. With the increase of the pitch of the six-point spiral bellows, the pressure drop and the resistance coefficient were both decrease.

Existing researches mostly take individual spiral structure and individual tubeline shape as the research object. This paper combines the spiral structure with the multi-head twisted structure. Numerical calculation was used to analyze the influence of the geometric parameters of the MTST on the flow resistance and heat transfer characteristics. Additionally, though using artificial neural network analysis, ratio of outside and inside diameter of the cross-section, number of twisted nodes and the number of twisted spiral tube heads were optimized to promote the comprehensive heat transfer performance.

Numerical simulation

Physical model

The structure of the MTST is shown in fig. 1. The main parameters of the MTST structure include the spiral diameter, D , and the pitch, H . Every 360 twisted degrees of the MTST is called a twisted node, and the number of twisted nodes is represented by L . The cross-sectional shape of the MTST is shown in fig. 2. The cross-sectional shape is composed of circular lines distributed at different circumferential angles and curves tangent to the circle. The a is the diameter of the outer circle of the section, b – the diameter of the inner circle of the section, n – the number of twisted spiral tube heads, and r – the diameter of the head. The outer diameter, a , is a fixed value of 25 mm, and the inner diameter, b , changes with the

change in the head diameter, r . The physical model shown in figs. 1 and 2 is a four-head twisted spiral tube, and the distribution angle of the different round heads is 90° . The wall surface of the MTST adopts a copper tube with a wall thickness of 1 mm.

Boundary conditions and governing equation

The working fluid is water. The Reynolds number range of fluid-flow in the MTST is 5000-35000. The initial velocity corresponding to the flow inlet is calculated according to the Reynolds number and hydraulic diameter. The inlet temperature of fluid is 303.15 K, and the wall surface is a fixed temperature of 333.15 K. The flow outlet is set as a pressure outlet, and the ambient pressure is maintained at atmospheric pressure. To simplify the calculation, the Prandtl number of water is 4, which is determined by the average value of the inlet temperature and the wall surface temperature.

The continuous equation of fluid-flow is as follows, where ρ and u are the density and inlet velocity of working fluid, respectively. The t is time, and u_i represents the velocity components along x_i :

$$\frac{\partial(\rho u_i)}{\partial x_i} = 0 \tag{1}$$

The momentum equation of fluid-flow is:

$$\frac{\partial}{\partial t}(\rho u_i) + \frac{\partial}{\partial x_j}(\rho u_i u_j) = -\frac{\partial P}{\partial x_j} + \frac{\partial}{\partial x_j} \left[\mu \left(\frac{\partial u_i}{\partial x_j} \right) + \frac{\partial u_j}{\partial x_i} - \frac{2}{3} \delta_{ij} \frac{\partial u_k}{\partial x_k} \right] + \frac{\partial}{\partial x_j} (-\rho \overline{u'_i u'_j}) \tag{2}$$

The energy equation of fluid-flow is:

$$\frac{\partial}{\partial x_i} [u_i (\rho E + P)] = \frac{\partial}{\partial x_i} \left[\left(\lambda + \frac{C_p \mu_t}{Pr_t} \right) \frac{\partial T}{\partial x_j} + \mu u_i \left(\frac{\partial u_i}{\partial x_j} + \frac{\partial u_j}{\partial x_i} - \frac{2}{3} \sigma_{ij} \frac{\partial u_k}{\partial x_k} \right) \right] \tag{3}$$

where T is temperature, E – the total energy, and C_p – the the specific heat:

$$E = \frac{C_p T - P}{2} + \frac{\rho + u^2}{2} \tag{4}$$

Based on the original Reynolds average Navier-Stokes equation, the $k-\varepsilon$ model introduces equations related to turbulent kinetic energy, k , and turbulent energy dissipation rate, ε , to simulate the turbulent process and predict the flow state of bending and rotation. In $k-\varepsilon$ models, the standard $k-\varepsilon$ model is widely used to simulate the boundary-layer of flow. However, the eddy viscosity value calculated by the standard $k-\varepsilon$ model in high shear rate and severe flow conditions is often higher than the actual value. The realizable $k-\varepsilon$ model is more suitable for shear flow, boundary-layer flow on a flat plate, and flow in channels with pressure



Figure 1. The MTST

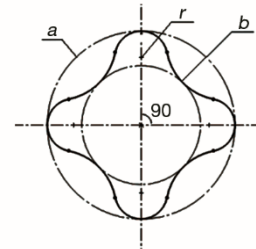


Figure 2. Section shape of four-head twisted spiral tube

gradients. The flow process involves curved streamlines, vorticity, and extreme rotation. Thus, this study uses the realizable $k-\varepsilon$ model for calculation [18].

Data calculation

The average convective heat transfer coefficient, h , represents the convective heat transfer rate per unit heat transfer area under unit temperature difference. It is defined:

$$h = \frac{q}{\Delta T} \quad (5)$$

where q is heat flux generated by the fluid-flow process and ΔT – the logarithmic mean temperature difference, which is defined:

$$\Delta T = \frac{(T_w - T_{f,in}) - (T_w - T_{f,out})}{\ln\left(\frac{T_w - T_{f,in}}{T_w - T_{f,out}}\right)} \quad (6)$$

where T_w is the average temperature along the wall surface and $T_{f,in}$ and $T_{f,out}$ are the average inlet fluid temperature and average outlet fluid temperature respectively. The Nusselt number are surface-averaged values which are calculated:

$$\text{Nu} = \frac{hd}{\lambda} \quad (7)$$

where λ is the thermal conductivity of the working fluid which represents the ability of a material to transfer heat. The friction coefficient, f , is the dimensionless number that characterizes the flow resistance in the flow process:

$$f = \frac{2\Delta P d}{\rho u^2 C} \quad (8)$$

where ΔP is the pressure change of the fluid-flowing in the tube and C – the length of the spiral tube. The performance evaluation criterion (PEC) [19] is used to measure the degree of energy saving and enhanced heat transfer of the enhanced heat transfer structure compared with the smooth tube. The expression of PEC is:

$$\text{PEC} = \frac{\text{Nu}_{mh}}{\text{Nu}_s} \frac{1}{\left(\frac{f_{mh}}{f_s}\right)^3} \quad (9)$$

where Nu_{mh} , f_{mh} , and Nu_s , f_s are the Nusselt number and friction coefficient of the MTST and the spiral smooth tube with the same hydraulic diameter, respectively. When the PEC value is greater than 1, the enhanced heat exchange structure can improve the heat exchange efficiency on the basis of saving pump power.

Grid independent and model validation

The grids of the MTST are shown in fig. 3. The grids of the MTST adopt the tetrahedral unstructured method. The grids of tube wall are refined by adding a boundary-layer, and the number of boundary-layers is seven. The fluid temperature distribution in the tube is used as the standard to measure independent grids. Figure 4 shows the temperature distribution in the tube when the number of grids is 445082, 651268, 1072942, 1193858, and 1315984. As shown in fig. 4, as the number of grids increases, the fluid temperature rises slightly. When the number of grids is greater than 1.07 million, the deviation in temperature change is less than 1%. The numerical calculation is performed with 1.07 million grids, considering the calculation accuracy and calculation time.

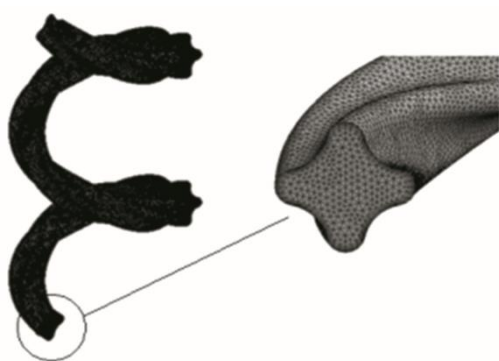


Figure 3. Grids of multi-head twisted spiral tube

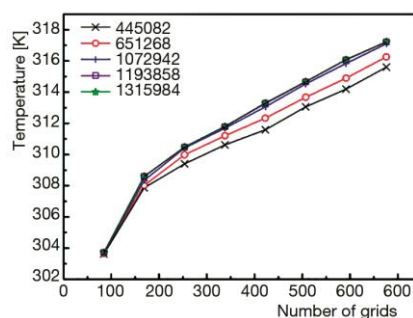


Figure 4. Grid independent validation

The model validation are conducted with the available empirical formulas on turbulent flow and heat transfer in smooth spiral tube. The Nusselt number and friction coefficient of a smooth spiral tube with $D = 100$ mm, $H = 125$ mm, and equivalent diameter $d = 25$ mm are calculated. The calculation results are compared with the empirical formulas of Roger and Mayhew [20] and Ito [21]. The calculation results are compared with the empirical formulas [20, 21] are shown in tab. 1. As shown in figs. 5 and 6, the calculation results of Nusselt number and friction coefficient are

Table 1. Empirical formula for comparison

Empirical formulas	
[20]	$Nu = 0.023 Re^{0.8} Pr^{0.4} (d/D)^{0.1}$
[21]	$F = 0.076 Re^{-0.25} + 0.00725 (d/D)^{0.5}$

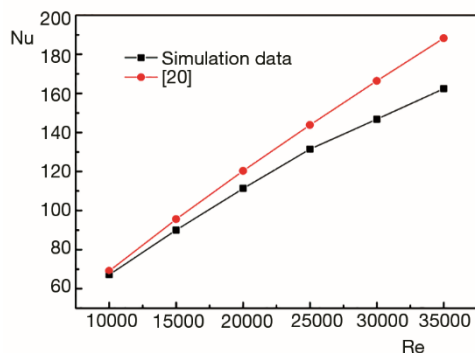


Figure 5. Comparison of Nusselt number

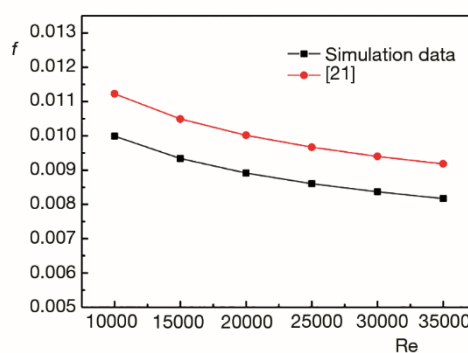


Figure 6. Comparison of friction coefficient

consistent with the calculation results of the Roger formula and Ito formula. The maximum deviations are 15.898% and 12.362% which indicates that the calculation results are reliable.

Results and discussion

Influence of the ratio of outside and inside diameter on the flow and heat transfer characteristics

The twisted tube structure and the spiral structure generate a disturbing effect on the fluid-flow. Figure 7 shows the fluid-flow velocity distribution in the four-head twisted spiral tube with different ratio of outside and inside diameter of the cross-section at the same position under the condition of a Reynolds number of 15000. The velocity of the fluid at the head is slower than that of the mainstream area. A violent swirling flow is generated in the mainstream area within the inner diameter of the cross-section.

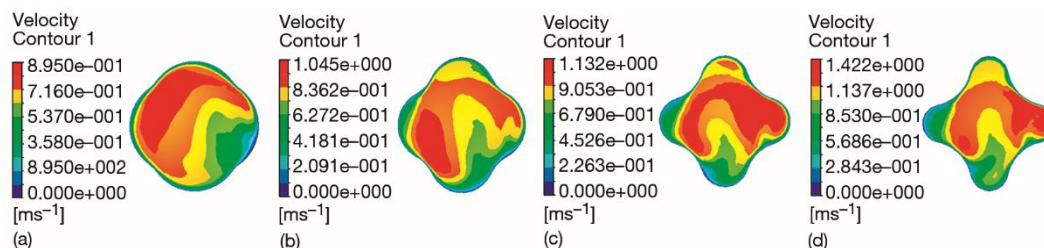


Figure 7. Velocity distribution under different section diameter ratio; (a) $a/b = 25/17.5$, (b) $a/b = 25/15$, (c) $a/b = 25/22.5$, and (d) $a/b = 25/20$

Figures 8 and 9 show the changes in the Nusselt number and friction coefficient of the four-head twisted spiral tube, respectively, under the conditions of different ratio of outside and inside diameter of the cross-section. Figure 8 shows that the Nusselt number of the four-head twisted spiral tube increases with the increase in Reynolds number. In addition, the Nusselt number increases with the increase in the ratio of outside and inside diameter of the cross-section. The Nusselt number increased by 26.4% on the average when the ratio of outside and inside diameter of the cross-section is 25/22.5-25/15.

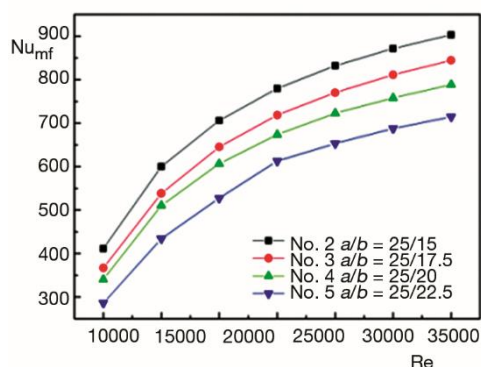


Figure 8. Nusselt number under different section diameter ratios

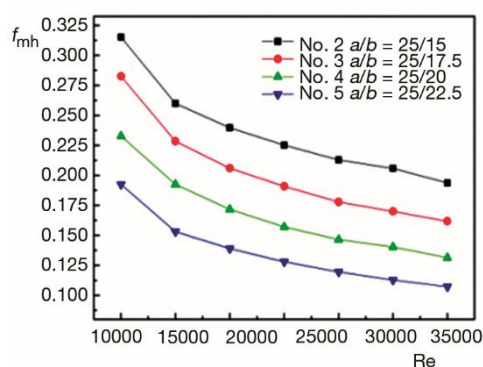


Figure 9. Coefficient of friction under different section diameter ratios

Compared with fig. 7, a strong swirling flow generated from the curvature wall takes the fluid continuously and flushes the tube wall to take away heat. The violent fluid mixing and secondary flow effectively destroy the heat transfer boundary-layer. Thus, the heat exchange efficiency is significantly improved.

Figure 9 shows that the friction coefficient in the four-head twisted spiral tube also increases with the increase in the ratio of outside and inside diameter of the cross-section. When the ratio of the outside and inside diameter of the cross-section is 25/22.5-25/15, the friction coefficient increases by 76.59% on the average. The twisted tube causes an increase in flow pressure dissipation due to the flow resistance caused by the violent fluid mixing.

Influence of the number of twisting nodes on the flow and heat transfer characteristics

Figure 10 shows the fluid-flow velocity distribution in a four-head twisted spiral tube with different twisting nodes at the same position under the condition of 15000 Reynolds number. The figure also shows that as the number of twisted nodes increases, the flow velocity of the liquid flow at the head of the twisted spiral tube is significantly reduced. The fluid gathers at the head position under the twisting effect. The fluid-flow concentrates on the main flow area, where the inner diameter of the cross section is located.

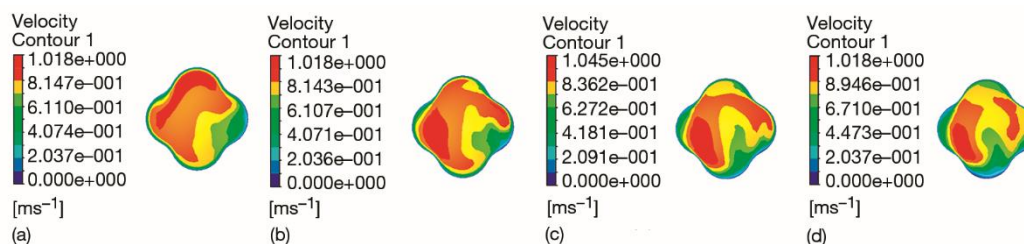


Figure 10. Velocity distribution under different number of twisted nodes; (a) $L = 2$, (b) $L = 4$, (c) $L = 6$, and (d) $L = 8$

Figure 11 shows the variation of the Nusselt number in the four-head twisted spiral tube with different twisted nodes. Figure 11 shows that under the same Reynolds number, the Nusselt number increases with the number of twisted nodes. When the number of twisted nodes is 2 to 8, the Nusselt number increases by an average of 9.05%. The increase in the number of twisted nodes increases the twisted degree of the twisted spiral tube. Thus, the intensity of the vortex flow increases and becomes disordered.

Figure 12 shows the variation of the friction coefficient of the four-head twisted spiral tube with different twisting pitches. Figure 8 shows that the friction coefficient increases with the number of twisted nodes. When the number of twisted nodes is 2 to 8, the friction coefficient increases by 32.08% on the average. When the number of twisted nodes is increased from 6 to 8, the friction coefficient of the four-head twisted spiral tube increases significantly. The fluid-flow at the edge of the tube was slightly stagnated when the number of twisted nodes increased to 8. Therefore, the pressure loss of fluid-flow is significantly increased.

Influence of twisted structure on PEC

The PEC is used to measure the degree of enhanced heat transfer. Figure 13 shows the PEC variation of twisted spiral tubes with different ratios of outer and inner diameters.

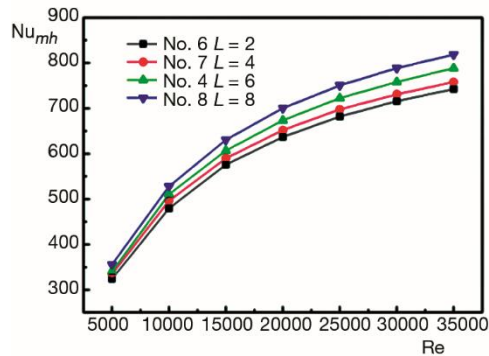


Figure 11. Nusselt number under different different numbers of twisted nodes

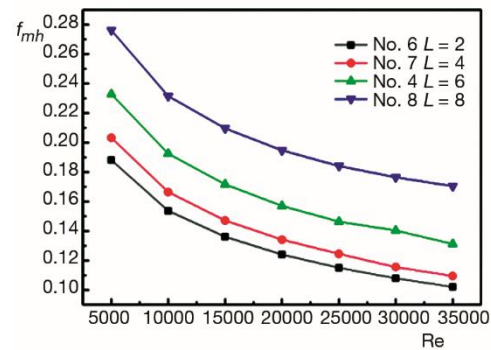


Figure 12. Coefficient of friction under different numbers of twisted nodes

When a/b is 25/22.5, the PEC of the twisted spiral tube is the highest, and the PEC can reach up to 1.22 of the spiral smooth tube with the same hydraulic diameter.

Figure 14 shows the PEC of different numbers of twisted nodes. The figure also shows that the PEC of the twisted spiral tube is the highest when $L = 4$. When the number of twisting nodes is 8, the PEC of the twisted spiral tube is worse than that of the spiral smooth tube with the same hydraulic diameter because the number of twisted nodes has a greater effect on pressure drop than heat transfer coefficient. The enhancement of the heat transfer efficiency by the increase in the number of twisted nodes cannot compensate for the pressure loss, decreasing in its overall performance.

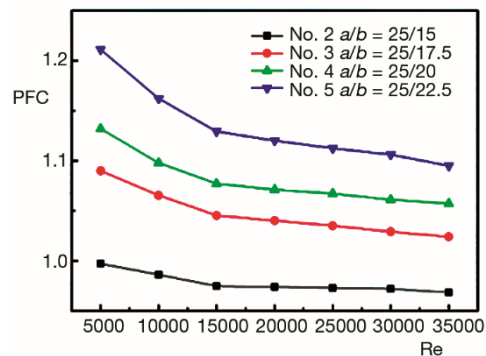


Figure 13. The PEC under different section diameter ratio

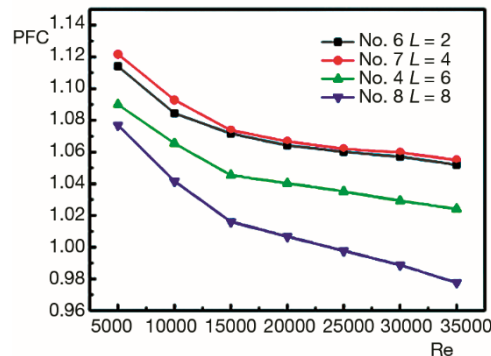


Figure 14. The PEC under different number of twisted nodes

Influence of the number of twisted spiral tube heads on the flow and heat transfer characteristics

Figure 15 shows the fluid-flow velocity distribution in the twisted spiral tube under. The increase in the number of twisted spiral tube heads strengthens the twisting degree of the twisted spiral tube to a certain extent. As shown in the figure, when the number of heads of the twisted spiral tube increases, more fluid is induced to the head area, and the main flow area in the tube produces evident vortex.

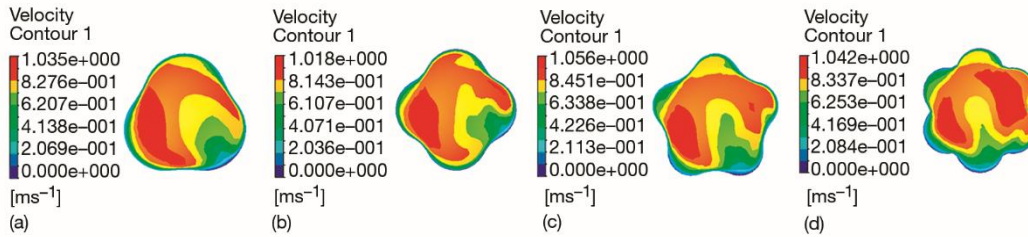


Figure 15. Velocity distribution under different number of twisted spiral tube heads; (a) $n = 3$, (b) $n = 4$, (c) $n = 5$, and (d) $n = 6$

Influence of the number of twisted spiral tube heads on the flow and heat transfer characteristics

Figure 16 shows the variation of the Nusselt number under different twisted spiral tube heads. As the Reynolds number increases, the Nusselt number of the twisted spiral tube with a larger number of twisted spiral tube heads increases faster. The Nusselt number increased by 7.49% on the average when the number of twisted spiral tube heads is 3 to 6. The vortex intensity in the mainstream area is strengthened by the increase in the number of twisted spiral tube heads. The fluid mixing caused by the vortex leads to more effective thermal boundary-layer destruction, and the Nusselt number increases.

Figure 17 shows the variation of friction coefficient under different numbers of twisted spiral tube heads. As the number of twisted spiral tube heads increases, the friction coefficient increases. When the number of twisted spiral tube heads is 3 to 5, the friction coefficient increases by an average of 30.39%. The vortex generated by the increase in the number of twisted spiral tubes greatly increases the pressure loss during fluid-flow.

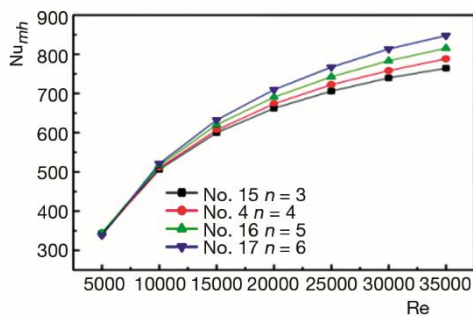


Figure 16. Nusselt number under different number of twisted spiral tube heads

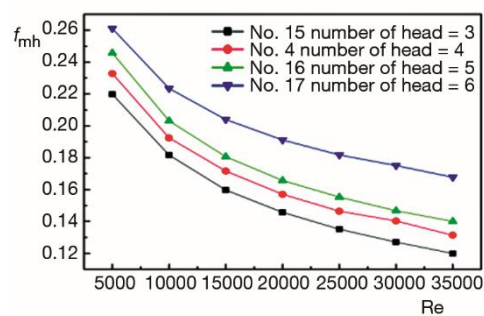


Figure 17. Coefficient of friction under different number of twisted spiral tube heads

The influence of the number of twisted spiral tube heads on PEC

The PEC of different twisted spiral tube heads is shown in fig. 18. The number of twisted spiral tube heads increases, and the PEC value decreases. When the number of spiral tube heads is 3, the comprehensive heat transfer performance of the twisted spiral tube is the highest, and the PEC can reach up to 1.121 of the spiral smooth tube with the same hydraulic radius. The increase in the number of spiral tube heads greatly affects the friction coefficient. Therefore, the increase in the number of twisted spiral tube heads reduces the PEC value.

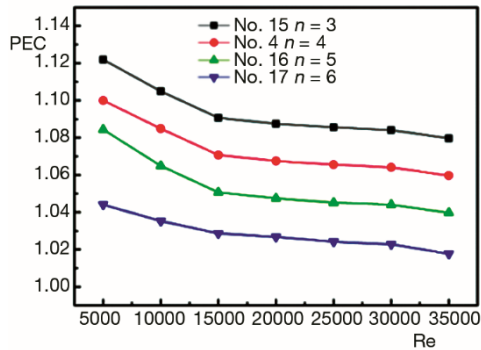


Figure 18. The PEC under different number of twisted spiral tube heads

Artificial neural network optimization

Establishment of artificial neural network model based on calculated data

Artificial neural network (ANN) is a machine learning model used for data classification or data prediction. Neurons mainly include input layer, hidden layer, and output layer. Each neuron has an activation function, which is used to count the number of neurons stimulated. In each layer, the set of neurons performs certain transformations on the input parameters and distribute these parameters to the next layer.

The input of the ANN model [22] is obtained from numerical calculation results. Under the condition that the spiral structure parameters remain unchanged ($H = 125$ mm, $D = 100$ mm), the ratios of the outside and inside diameters of the section, the number of twisted nodes, and the number of twisted spiral tube heads are selected as variables, as shown in fig. 19. The inlet Reynolds number is 15000, and the outputs of the two submodels are Nusselt number and friction coefficient. Some data are shown in tab. 2.

The input of the ANN model [22] is obtained

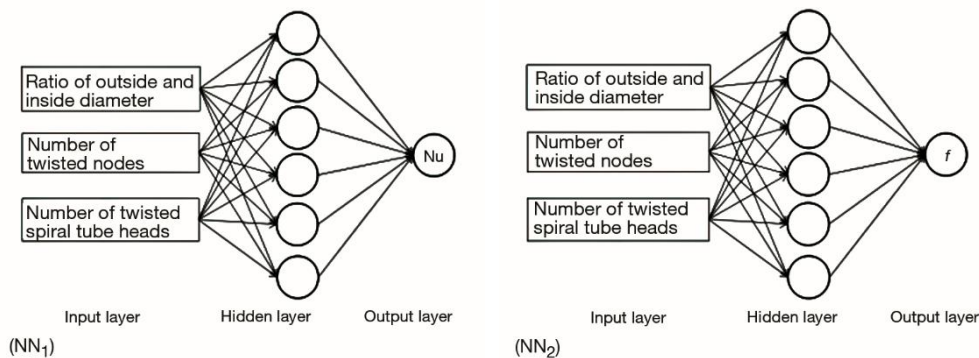


Figure 19. Scheme of neural network model

Table 2. Partial training data

Number	Ratio of outside and inside diameter	Number of twisted nodes	Number of twisted spiral tube heads	Nusselt number	Friction coefficient
1	25/22.5	1	8	382.653	0.06346
2	25/22.5	2	8	430.743	0.0645
3	25/22.5	3	8	546.723	0.07318
.....					
3988	25/15	8	2	754.559	0.458937
3989	25/15	9	2	778.153	0.474191
3990	25/15	10	2	803.096	0.483035

Establishment of neural network regression model

As shown in fig. 20, a higher fitting accuracy rate is obtained after the model is trained. In the training process, the fitting accuracy rates of NN₁ and NN₂ are 96.308% and 95.094%, respectively. In the verification process, the fitting accuracy rates of NN₁ and NN₂ are 97.409% and 99.358%, respectively. In the test process, the fitting accuracy rates of NN₁ and NN₂ are 97.643% and 94.114%, respectively. In the overall process, the fitting accuracy rates of NN₁ and NN₂ are 96.271% and 93.78%, respectively.

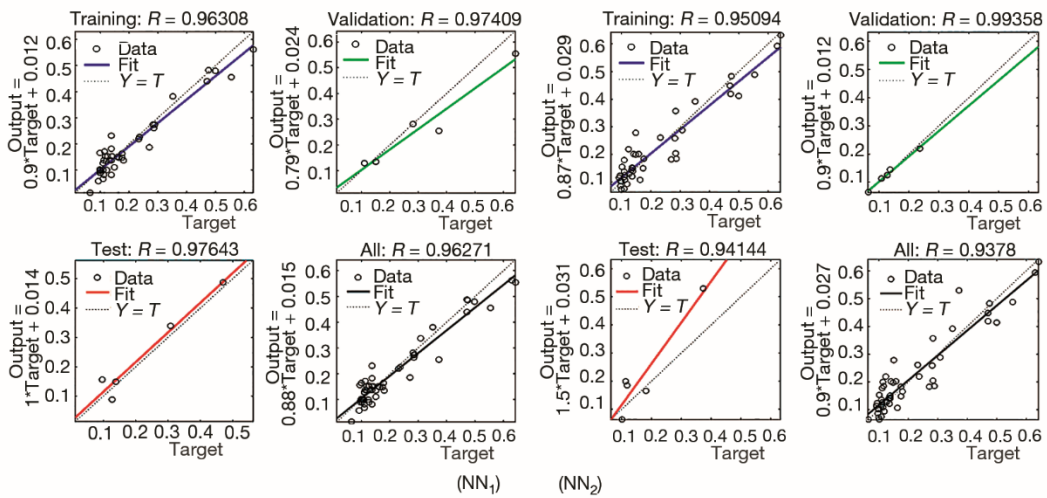


Figure 20. Regression performance

The deviation histograms of the two neural network submodels are shown in fig. 21. The error distributions of the two neural network models follow the Gaussian distribution rule, which proves the representativeness of the training data.

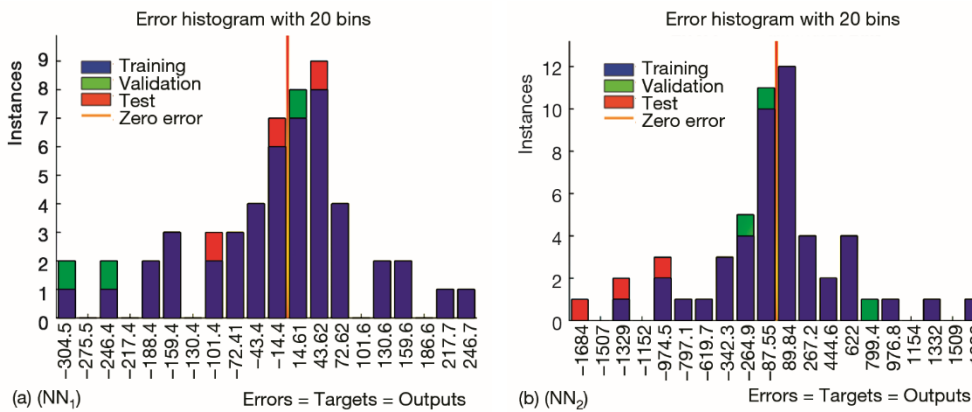


Figure 21. Error histogram

The ratio of outside and inside diameter of the cross-section (1.11, 1.12, ..., 1.67), the number of twisted nodes (1, 2, ..., 10), and the number of twisted spiral tube heads (2, 3, ..., 8) are regarded as variables for data prediction. The number of data is $57 \cdot 10 \cdot 7 = 3990$. An opti-

mal structure is selected for all calculation data on the basis of a smaller friction coefficient to obtain a larger Nusselt number. The PEC is calculated to determine enhanced heat transfer performance of optimal structure. When the ratio of the outside and inside diameters, the number of twisted nodes, and the number of twisted spiral tube heads are 1.4, 3, and 3, respectively, the optimal structure is the best.

Table 3 shows the comparison between the best calculation data and the worst uniformity data after ANN model optimization. The table shows that the worst structure is more complicated whose heat transfer efficiency is higher. Its Nusselt number is only increased by 8.9% relative to the optimal structure. However, its friction coefficient is increased by 56.18% compared with the optimal structure. The PEC of the best optimal structure is increased by 36.89% compared with the worst structure. Therefore, the optimization of parameters can improve the *bucket effect* by improving the worst-performing monomer. The overall enhanced heat transfer performance has been improved.

Table 3. Performance comparison

Comparison of best and worst structure						
	Ratio of outside and inside diameter	Number of twisted nodes	Number of twisted spiral tube heads	Nusselt number	Friction coefficient	PEC
Worst	1.67	5	6	747.430	0.1832	1.066
Best	1.4	3	3	685.886	0.1173	1.849
Optimization	–	–	–	8.9%	56.18%	36.89%

Conclusions

Numerical analysis of the flow and heat transfer mechanism in the MTST is carried out. The vortex generated by the twisted structure and the secondary flow generated by the spiral structure effectively destroy the flow boundary-layer. The heat exchange efficiency of the MTST is significantly enhanced. In addition, the complex twisted flow structure increases the friction coefficient, thereby increasing the required pump power significantly.

The MTST has stronger comprehensive heat transfer performance than the spiral smooth tube. In the MTST, the Nusselt number increases as the Reynolds number increases, and the friction coefficient decreases as the Reynolds number increases. The Nusselt number and friction coefficient increase with the increase in the ratio of outside and inside diameter of the cross-section, the number of twisted nodes, and the increase in the number of twisted spiral tube heads.

The ANN model is used to optimize the ratio of outside and inside diameter of the cross-section (1.11, 1.12, ..., 1.67), the number of twisted nodes (1, 2, ..., 10), and the number of twisted spiral tube heads (2, 3, ..., 8). A total of 3990 sets of data are trained, tested, and verified. When the ratio of outside and inside diameter of the cross-section is 1.4, the number of twisted nodes is 3, and the number of twisted spiral tube heads is 3. In addition, the PEC of the MTST can reach the best under the condition of the same hydraulic diameter. The PEC value can reach 1.849.

References

- [1] Liu S, Sakr M. A Comprehensive Review on Passive Heat Transfer Enhancements in Pipe Exchangers, *Renewable and Sustainable Energy Reviews*, 19 (2013), Mar., pp. 64-81

- [2] Bergles, A. E., Heat Transfer Enhancement - The Encouragement and Accommodation of High Heat Fluxes, *Journal of Heat Transfer-Transactions of the ASME*, 119 (1995), 1, pp. 8-19
- [3] Mishra P, Gupta S. N., Momentum Transfer in Curved Pipes. 2. Non-Newtonian Fluids, *Industrial & engineering chemistry process design and development*, 18 (1979), 1, pp. 137-142
- [4] Cioncolini, A, Santini, L. On the Laminar to Turbulent Flow Transition in Diabatic Helically Coiled Pipe Flow, *Experimental Thermal and Fluid Science*, 30 (2006), 7, pp. 653-661
- [5] Gupta, R., et al., Laminar Flow in Helical Coils: A Parametric Study, *Industrial & Engineering Chemistry Research*, 50 (2011), 2, pp. 1150-1157
- [6] Bozzoli, F., et al., Effect of Wall Corrugation on Local Convective Heat Transfer in Coiled Tubes, *International Journal of Heat and Mass Transfer*, 101 (2016), Oct., pp. 76-90
- [7] Dong, X., et al. Experimental Research on Heat Transfer and Flow Resistance Properties in Spiral Twisted Tube Heat Exchanger, *Applied Thermal Engineering*, 176 (2020), July, 115397
- [8] Kongkai-paiboon, V., et al., Effects of Spiral Start Number and Depth Ratio of Corrugated Tube on Flow and Heat Transfer Characteristics in Turbulent Flow Region, *Journal of Mechanical Science and Technology*, 33 (2019), 8, pp. 4005-4012
- [9] Rainieri, S., et al., Compound Convective Heat Transfer Enhancement in Helically Coiled Wall Corrugated Tubes, *International Journal of Heat and Mass Transfer*, 59 (2013), Apr., pp. 353-362
- [10] Wang, W., et al., Influence of Geometrical Parameters on Turbulent Flow and Heat Transfer Characteristics in Outward Helically Corrugated Tubes, *Energy Conversion and Management*, 136 (2017), Mar., pp. 294-306
- [11] Wang, W., et al., Numerical Study on Fully-Developed Turbulent Flow and Heat Transfer in Inward Corrugated Tubes with Double-Objective Optimization, *International Journal of Heat and Mass Transfer*, 120 (2018), May, pp. 782-792
- [12] Akbarzadeh, M., et al., Influences of Corrugation Profiles On Entropy Generation, Heat Transfer, Pressure Drop, and Performance in a Wavy Channel, *Applied thermal engineering*, 116 (2017), Apr., pp. 278-291
- [13] Khoshvaght-Aliabadi, M., et al., Empirical and Numerical Assessments on Corrugated and Twisted Channels as Two Enhanced Geometries, *International journal of mechanical sciences*, 157-158 (2019), July, pp. 25-44
- [14] Tang, X., et al., Experimental and Numerical Investigation of Convective Heat Transfer and Fluid-flow in Twisted Spiral Tube, *International Journal of Heat and Mass Transfer*, 90 (2015), Nov., pp. 523-541
- [15] Yang, S., et al., Experimental Study on Convective Heat Transfer and Flow Resistance Characteristics of Water Flow in Twisted Elliptical Tubes, *Applied Thermal Engineering*, 31 (2011), 14-15, pp. 2981-2991
- [16] Kareem, Z. S., et al., Passive Heat Transfer Enhancement Review in Corrugation, *Experimental Thermal and Fluid Science*, 68 (2015), Nov., pp. 22-38
- [17] Jin, Z., et al., CFD Analysis on Flow Resistance Characteristics of Six-Start Spirally Corrugated Tube, *International Journal of Heat and Mass Transfer*, 103 (2016), Dec., pp. 1198-1207
- [18] Zaboli, M., et al., Numerical Evaluation of the Heat Transfer and Fluid-flow in a Corrugated Coil Tube with Lobe-Shaped Cross-Section and Two Types of Spiral Twisted Tape as Swirl Generator, *Journal of Thermal Analysis and Calorimetry*, 147 (2020), Sept., pp. 999-1015
- [19] Han, H., et al., Multi-Objective Shape Optimization of Double Pipe Heat Exchanger with Inner Corrugated Tube Using RSM Method, *International journal of thermal sciences*, 90 (2015), Apr., pp. 173-186
- [20] Rogers, G. F. C., Mayhew, Y. R., Heat Transfer and Pressure Loss in Helically Coiled Tubes with Turbulent Flow, *International Journal of Heat and Mass Transfer*, 7 (1964), 11, pp. 1207-1216
- [21] Ito, H., Friction Factors for Turbulent Flow in Curved Pipes, *Journal of Basic Engineering*, 81 (1959), 2, pp. 129-134
- [22] Verma, T. N., et al. ANN: Prediction of an Experimental Heat Transfer Analysis of Concentric Tube Heat Exchanger with Corrugated Inner Tubes, *Applied Thermal Engineering*, 120 (2017), June, pp. 219-227